Journal of Marine Research, 49, 53–73, 1991

Nonlinear general circulation of an ocean model driven by wind with a stochastic component

by Annalisa Griffa[1] and Sergio Castellari[1]

ABSTRACT

The effects of the stochastic component of the large-scale wind on the climatological mean of the nonlinear ocean circulation are studied, using a set of numerical solutions for the single-layer, quasi-geostrophic equation in a closed basin with a flat bottom. In the absence of a steady wind, the purely stochastic wind is found to drive the solutions toward a nonlinear mean flow similar to that of the free system (i.e. without forcing and dissipation). This equilibrium mean flow (Fofonoff flow), is predicted by statistical mechanics and is characterized by a westward interior closed by inertial boundary layers along the coast. When a steady component of the wind is present, the effects of the stochastic wind depend on the geometry of the steady wind. If the steady wind is compatible with Fofonoff flow, the stochastic wind tends to reinforce the Fofonoff-like mean solution obtained with the steady wind alone. When the steady wind opposes Fofonoff flow, the contribution of the stochastic wind does not increase the energy of the mean solution, but instead tends to change the spatial structure of the mean flow. An example of steady wind opposing Fofonoff flow is the classical double-gyre wind, often used to represent the realistic mean wind in mid-latitude ocean regions. We study the double-gyre wind case in detail. The stochastic wind is found to weaken the recirculating regions and the meandering jet between the two gyres, and the homogenization of potential vorticity in the recirculations is inhibited. These changes are explained in terms of increased mixing of the probability density in phase space due to the stochastic wind, causing an increased tendency toward the equilibrium state predicted by statistical mechanics.

1. Introduction

In a recent paper, Griffa and Salmon (1989, GS in the following) apply an approach based on the theory of equilibrium statistical mechanics to the study of the nonlinear general circulation of an ocean driven by steady wind. In the present paper, the results of GS are generalized to the study of the circulation driven by a superposition of steady wind and large-scale stochastically fluctuating wind with zero mean. In particular, we investigate the influence of the fluctuating component of the wind on the climatological mean of the ocean circulation through the nonlinear processes of rectification. Two independent observations contribute to make this topic very relevant: (a) the fluctuating component of the wind driving the ocean

1. University of Miami, Rosenstiel School of Marine and Atmospheric Science, 4600 Rickenbacker Causeway, Miami, Florida, 33149, U.S.A.

circulation is, over large regions, more energetic than the steady component, and (b) the nonlinear dynamics play an important role in the general circulation of the ocean, especially in the highly energetic regions close to the western boundary.

The effects of atmospheric fluctuations on the ocean circulation have been studied extensively in the literature, especially with regard to the generation of open ocean mesoscale variability or low frequency (annual or seasonal) variability (e.g. Muller and Frankignoul, 1981; Dewar, 1989; Greatbatch and Li, 1990). Less work has been devoted to the study of the effect of fluctuating winds on the mean circulation. Haidvogel and Rhines (1983) consider the rectified response of the ocean to spatially localized oscillatory wind-stress, whereas the response to large-scale time dependent wind has been studied by Veronis (1970, V70 in the following) and by Willebrand *et al.* (1980, WPP in the following). V70 considers the action of a fluctuating, single harmonic wind stress on a simple ocean model in a nonlinear regime characterized by high forcing and dissipation. He shows that a purely fluctuating wind with no steady component can generate a strong mean circulation, characterized by an anticyclonic gyre in the northern part of the basin and a cyclonic gyre in the southern part. V70 considers also the superposition of a fluctuating wind and a steady (single-gyre) wind. In this case, he finds that the mean ocean transport through the western boundary increases (perhaps double) because of the effect of the fluctuating wind. He concludes that "a serious underestimate of the transport may result if one works with time-average wind alone." A different conclusion is reached by WPP, who consider a different parameter range and a different, stochastically fluctuating, time-dependent wind. The WPP wind is more realistic than the V70 wind, as it is computed from twice-daily weather maps for a period of three years (Willebrand, 1978). The energy level considered by WPP, though, is probably too low, because of the severe smoothing in the data of the pressure field used to compute the geostrophic wind. WPP consider the case of purely stochastic wind, with no steady component. The regime of the ocean circulation obtained with this forcing is almost linear, but a rectified mean flow is observed to emerge, with a pattern similar to the one found by Veronis. The energy of the mean currents computed by WPP is very low, and because of this, WPP argue, in variance with Veronis, that rectified currents cannot alter in a significant way the mean flow determined by a steady wind alone. The works of V70 and WPP leave open a number of important questions. The action of the stochastic wind with a realistic energy level superimposed on a steady wind should be further investigated. In particular, the changes that the stochastic wind imparts on the mean solutions obtained with the steady wind alone, should be considered. The mean flow modifications cannot be predicted as a simple superposition of the contributions of the steady wind and the stochastic wind, because they depend on the nonlinear processes of eddy-mean flow interaction. Specific studies should then be performed, considering various geometries of the steady wind. The

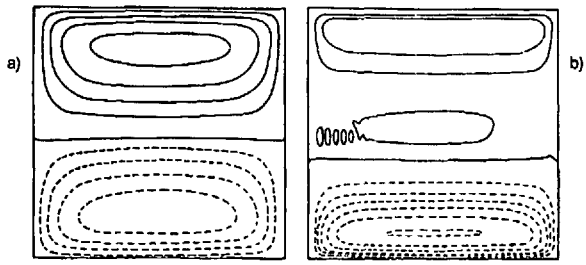

Figure 1. Average streamfunction of two nonforced nondissipative experiments with different initial conditions, from Griffa and Salmon (1989); (a) highly energetic experiment, Rossby number = 15.9×10^{-3}. The solution resembles Fofonoff flow; (b) less energetic experiment, Rossby number = 2.9×10^{-3}. The solution is still evolving, and the gyres are gradually expanding to fill the basin. The asymmetry between the northern and southern gyre is due to the positive value of the total vorticity in the initial conditions.

changes due to the stochastic wind in the mean solutions should be investigated not only in terms of total properties such as energy and transport, but also in terms of local dynamics and structure of the mean flows. These open questions motivate the present work and are addressed in the following.

In Section 2 we briefly summarize the approach taken by GS in the study of the nonlinear general circulation. The first step in GS is to analyze the nonlinear processes in the limiting case of an ocean with no forcing and no dissipation using the theory of equilibrium statistical mechanics (e.g., Holloway, 1986a). This theory predicts the equilibrium state (i.e. the final state) of the flow, due only to its nonlinear self-interactions. For a simple quasi-geostrophic, one-layer, flat bottom model of the ocean, statistical mechanics predicts (Salmon *et al.,* 1976) that the equilibrium state is characterized by a mean flow $\langle\psi\rangle$, called Fofonoff flow after Fofonoff (1954), characterized by a westward interior closed by inertial boundary layers along the coast, similar to Figure 1a. The meaning of the statistical mechanics prediction, put simply, is that given an initial condition characterized by a random eddy field, the eddies are expected to naturally organize themselves into a mean Fofonoff flow. GS verify this prediction with numerical simulations. As a successive step, GS introduce steady forcing and dissipation. It is shown that, even in the presence of forcing and dissipation, the nonlinearity still tends to drive the numerical solution toward the "natural" equilibrium state predicted by statistical mechanics, characterized by the mean Fofonoff flow. The actual success of this tendency turns out to be strongly dependent on the geometry of the wind stress.

In Section 3 and 4, we apply the results of GS to the study of numerical solutions of the quasi-geostrophic equation driven by winds with a stochastic component. The central idea (which has already been suggested by Holloway, 1986b) is that the fluctuating component of the wind always tends to drive the ocean circulation toward

a Fofonoff-like mean flow. The stochastic wind, in fact, reinforces the eddy field and consequently the nonlinear tendency toward the statistical mechanics equilibrium characterized by the Fofonoff mean. When there is no steady component of the wind, this tendency is free to emerge and the numerical solutions are characterized by a Fofonoff-like mean flow, completely maintained by the turbulent eddy field. When the wind also has a steady component, we argue that the action of the stochastic wind depends critically on the geometry of the steady wind. A general framework is provided to understand solutions corresponding to a wide range of steady wind geometries. Special attention is given to the case of the classical double-gyre wind (e.g. Holland, 1978), providing an ideal representation of the real mid-latitude wind.

The ocean model that we consider, quasi-geostrophic, one-layer with flat bottom, is extremely simple. This allows us to isolate and study the rectification processes due to the stochastic forcing alone. Many of the results that we obtain, though, are quite general and can be applied to more realistic models including those with bottom topography (Barnier and Le Provost, 1989).

2. Background

a. Equilibrium statistical mechanics. Solutions of the quasi-geostrophic equation in absence of forcing and dissipation. The method of equilibrium statistical mechanics has been applied successfully to many problems in geophysical fluid dynamics. It predicts the equilibrium states toward which finite-resolution models of macroscopic fluid systems would evolve in absence of forcing and dissipation. These equilibrium states are of interest, because they anticipate the role of the nonlinear interactions in realistic flows, subject to forcing and dissipation. Here we briefly summarize the results of the equilibrium theory applied to a quasi-geostrophic model of a flow in a closed basin. For a complete review of the theory and of the applications, the reader is referred to Kraichnan and Montgomery (1980), Salmon (1982) and Holloway (1986a).

The quasi-geostrophic equation for a one-layer ocean, with flat bottom and in a square basin is:

$$\begin{aligned} \partial q/\partial t + J(\psi, q) &= (1/\rho H)(\tau_o \operatorname{curl} \tau_s + \operatorname{curl} \tau_f) + D \\ q &= \zeta + f \\ \zeta &= \nabla^2 \psi \\ f &= f_o + \beta y \end{aligned} \tag{2.1}$$

where x, y are the Cartesian coordinates in the east and north direction respectively, $\psi(x, y, t)$ is the stream function, $\zeta(x, y, t)$ is the relative vorticity, $q(x, y, t)$ is the potential vorticity, f is the Coriolis parameter, ρ is the mass density, H is the constant depth, τ_o is a representative magnitude for the steady wind stress, $\tau_s(x, y)$ is the

normalized steady component of the zonal wind stress, $\tau_f(x, y, t)$ is the fluctuating stochastic component (with zero mean) of the zonal wind stress, and D is a dissipation operator. The boundary conditions are $\psi = 0$ at the coastal boundaries.

In absence of forcing and dissipation, $\tau_s = \tau_f = D = 0$, the dynamics (2.1) conserve the energy

$$E = \int\int_A (\nabla\psi)^2 \, dxdy \tag{2.2}$$

and the infinite hierarchy of momenta

$$Q_n = \int\int_a q^n \, dxdy \tag{2.3}$$

where A is the basin domain.

In order to apply the theory of equilibrium statistical mechanics, we consider a discrete numerical analogue of (2.1) with $\tau_s = \tau_f = D = 0$

$$d\psi_i/dt = F_i(\psi_1, \ldots, \psi_N) \qquad i = 1, N \tag{2.4}$$

where $\psi_i(t)$ is the value of the streamfunction of the i-th gridpoint or the amplitude of the i-th mode. The N-dimensional space spanned by the ψ_i represents a phase space where each point is a possible state of the system. We consider a probabilistic description of the system (2.4) introducing the joint probability distribution

$$P(\psi_1, \ldots, \psi_N, t)$$

of the ψ_i in an ensemble of realizations of (2.4).

If, as it is usually the case, the discretization (2.4) satisfies the Liouville Property $\Sigma_i \, \partial F_i/\partial\psi_i = 0$, then the equilibrium statistical mechanics applies. The equilibrium theory predicts that ensembles of solutions of (2.4) approach the equilibrium state defined by the macrocanonical probability density function

$$P_{eq}(\psi_1, \ldots, \psi_N) = \text{const.} \exp(-\lambda_o E - \sum_{j=1}^{\infty} \lambda_j Q_j). \tag{2.5}$$

where the constants λ_o, λ_j are determined by the mean initial values $\langle E \rangle$ and $\langle Q_j \rangle$.

In the fluid dynamical applications, moments Q_n with $n \geq 3$ are often ignored. Then (2.5) reduces to

$$P_{eq}(\psi_1, \ldots, \psi_N) = \text{const.} \exp(-\lambda_o E - \lambda_1 Q_1 - \lambda_2 Q_2) \tag{2.6}$$

that depends only on the energy $\langle E \rangle$, the total potential vorticity $\langle Q_1 \rangle$ and the total potential enstrophy $\langle Q_2 \rangle$ (for a discussion on the effects of the truncation of the higher moments $n \geq 3$, see e.g. Carnevale and Frederiksen (1987), CF in the following). P_{eq} (2.6) corresponds to a uniform probability distribution of system states

over hypersurfaces in phase space corresponding to fixed values of $\langle E \rangle$, $\langle Q_1 \rangle$ and $\langle Q_2 \rangle$. Introducing the ergodic hypothesis, P_{eq} can be considered as representative of the final (in time) state reached by the system (2.4). The nonlinear interactions, that drive the system toward the equilibrium state (2.6), can be thought of as a mechanism of spreading of P in the $\{\psi_i\}$ phase space, constrained by the conservation of $\langle E \rangle$, $\langle Q_1 \rangle$ and $\langle Q_2 \rangle$. P_{eq} corresponds to the maximum entropy state in the (ψ_i) space (e.g. Holloway, 1986a).

The expression (2.6) for P_{eq} is used to compute the statistics of the system (2.4) at the equilibrium. Salmon *et al.* (1976) show that the equilibrium mean flow $\langle \psi \rangle$ satisfies the discrete analogue of

$$\nabla^2 \langle \psi \rangle + \beta(y - y_o) = \alpha \langle \psi \rangle \tag{2.7}$$

where $\beta y_o = -f_o - \lambda_1/2\lambda_2$; $\alpha = \lambda_o/\lambda_2$. Eq. (2.7) states that the equilibrium mean flow is characterized by a linear relationship between $\langle \psi \rangle$ and $\langle q \rangle$. For realistic values of the energy, α is positive and solutions of (2.7) have a constant westward interior flow closed by inertial boundary layers (similar to Fig. 1a). The circulation is characterized by an anticyclonic gyre in the northern part of the basin and a cyclonic gyre in the southern part. The relative strength and the extension of the two gyres depend on the initial value of the total vorticity and therefore on Q_1. These mean flows are called Fofonoff flows. Note that the linear relationship between $\langle \psi \rangle$ and $\langle q \rangle$ in (2.7) is a direct consequence of the truncation of the higher moments $n \geq 3$ in (2.5). Nonlinear modifications of the $\langle \psi \rangle - \langle q \rangle$ relationship would arise if one would retain higher invariants. The issue of the relative importance of quadratic and higher invariants is still open and debated in the literature (CF; Vallis *et al.*, 1989).

In order to test the prediction of equilibrium statistical mechanics, GS study the numerical solutions of (2.1) with zero wind stress and $D = D_{ev}$, where D_{ev} is a scale selective eddy viscosity that represents the effects of the unresolved small scales. The anticipated potential vorticity (APV) scheme (Sadournay and Basdevent, 1985) is used, that simulates the phenomenology of the two-dimensional inertial range by dissipating enstrophy and not energy. Note that the introduction of D_{ev} (or of any other eddy viscosity) invalidates the Liouville property that is one of the main assumptions of statistical mechanics. The use of an eddy viscosity in simulations that tend to assess the validity of equilibrium statistical mechanics needs then to be discussed and justified. To understand the effects of D_{ev} on the equilibrium states of the system, consider the following argument. The general tendency of the nonlinear interactions, even in the presence of D_{ev}, is characterized by an increase of the P mixing in phase space (and therefore of the entropy) which gives rise to a continuous transfer of enstrophy at small scales (e.g. Holloway, 1986a). In a numerical simulation, the enstrophy cascade is arrested at the highest wavenumber k_{max} corresponding to the grid size. The excess of enstrophy that tends to pile up at k_{max} is constantly removed by D_{ev}. Strictly speaking then, it is expected that the solutions tend toward a

minimum enstrophy state, rather than toward the maximum entropy state predicted by statistical mechanics. On the other hand, it can be shown (Bretherton and Haidvogel, 1976) that the minimum enstrophy states of the system are characterized by quasi-steady solutions with the same Fofonoff structure (2.7) as the time-averaged solutions found for the maximum entropy states. Conceptually this is not surprising as the convergence toward the minimum enstrophy states can be explained in terms of maximization of the entropy. The following argument illustrates the basic ideas (a rigorous discussion can be found in CF and GS). Consider a free system (without D_{ev}) truncated at the maximum wavenumber $k_{max} = k^*$. The enstrophy will tend to pile up at k^*. If the resolution of the system is increased by increasing the maximum wavenumber k_{max}, the enstrophy cascades from k^* to higher wavenumbers. One can imagine that the limit of infinite resolution for the free system is reached by further increasing k_{max}, and therefore by constantly removing enstrophy from the smallest scales. In this infinite resolution limit the maximum entropy state of the free system corresponds to a minimum enstrophy state, characterized by a very sharp Fofonoff mean flow. We expect then that the solutions obtained with D_{ev} will exhibit the same strong Fofonoff mean flow as the solutions without D_{ev} and with a much higher resolution.

All the analyzed solutions, starting from various random initial conditions, appear to converge toward an equilibrium state characterized by a time-averaged Fofonoff flow. The pathway of approach to the Fofonoff flow, turns out to be dependent on the energy of the initial conditions. If the total energy E of the initial conditions is (unrealistically) high, two mean gyres appear quite early in the evolution, well defined over the whole basin. The solutions quickly converge to a Fofonoff mean flow (Fig. 1a). If the energy is realistically small (Rossby number $R = u_{rms}/\beta L^2 \ll 1$, where L is the basin scale and u_{rms} is the r.m.s. velocity), instead, the two gyres are initially confined close to the zonal boundaries and the solutions pass through a sequence of states in which the inertial gyres gradually expand to fill the basin (Fig. 1b). Notice that in the interior of the gyres in Fig. 1b, the relationship between $\langle\psi\rangle$ and $\langle q\rangle$ is linear, as it is characteristic of the Fofonoff flow (2.7). The time T_{eq} necessary to completely fill the basin and reach the Fofonoff equilibrium state is very long compared to the advection time scale L/u_{rms}. We expect that the solution characterized by zonally confined gyres will play an important role in the presence of forcing and dissipation. The dissipation, in fact, introduces a time scale which is, in general, shorter than the time T_{eq} required to reach the exact Fofonoff state. As a consequence, the role of nonlinear interactions in the forced and dissipative cases will be to move the system toward states like those observed in Fig. 1b.

b. Solutions with steady forcing and dissipation. GS use the results summarized in 2a to interprete numerical solutions of (2.1) obtained in the presence of steady forcing ($\tau_s \neq 0$, $\tau_f = 0$) and dissipation. They consider a dissipation operator D sum of the

eddy viscosity D_{ev} plus a bottom drag with coefficient ϵ, $D = D_{ev} - \epsilon\zeta$. The bottom drag provides the mechanism of energy dissipation, whereas the eddy viscosity parameterizes the action of the unresolved scales. All the solutions are nonlinear and characterized by small forcing and dissipation (Rossby number $R \ll 1$, Ekman number $Ek \ll 1$).

The main conclusion of GS is that, even in the presence of forcing and dissipation, the nonlinearity still tends to drive the solutions toward the equilibrium state characterized by the Fofonoff flow (2.7). The equilibrium solutions of the forced and dissipative system (2.1) can be thought of as a balance between the nonlinearity, which tends to drive the solutions toward the equilibrium characterized by the Fofonoff flow, and the wind forcing and the bottom drag, which impose limits on this tendency. To understand how forcing and dissipation can oppose the Fofonoff flow, consider the time average of (2.1) at equilibrium:

$$\nabla(\langle u\rangle\langle q\rangle) + \nabla(\langle u'q'\rangle) = (\tau_o/\rho H)\,\mathrm{curl}\,\tau_s + \langle D\rangle \tag{2.8}$$

where the primes denote the departures from the time average. The integral of (2.8) over the area enclosed by a mean streamline $\langle\psi\rangle$ = const. yields

$$\oint\langle u'q'\rangle n\,dr = (\tau_o/\rho H)\oint\tau_s\,dr - \epsilon\oint\langle u\rangle\,dr \tag{2.9}$$

where dr is the counterclockwise displacement around the mean streamline and n is the outward unit normal. The dissipation term in (2.9) is approximated as $D = -\epsilon\zeta$ because (as verified numerically by GS) the bottom drag is always higher than the eddy viscosity in the local balances, by at least one order of magnitude.

If the solutions would reach a steady state, then (2.9) would have to be satisfied on every closed streamline, with the eddy flux of potential vorticity on the left-hand side set equal to zero. GS say that the wind is "compatible" with the Fofonoff flow when the two terms on the right-hand side of (2.9) nearly balance, with $\langle u\rangle$ being the mean velocity in the hypothetical Fofonoff state. When, instead, the right-hand side balance is not possible on Fofonoff streamlines, the wind is said to be incompatible with Fofonoff flow.

The numerical solutions of (2.1) are found to be very different depending on whether the wind is compatible with Fofonoff flow or not. When the wind is compatible with the Fofonoff flow, then the nonlinearity is able to succeed in driving the solution toward a Fofonoff-like state. The equilibrium solutions resemble Fofonoff flow, are energetic and nearly steady. When, on the other hand, the wind opposes the Fofonoff flow, the nonlinearity cannot succeed in pushing the wind-driven system very close to a Fofonoff state. The solutions are then turbulent, with weak mean flows and low energy contents. An example of wind compatible with Fofonoff solution is the classical single gyre pattern, $\tau_s = -\cos(\pi y/L)$, corresponding to a system of trade winds on $y < L/2$ and westerlies on $y > L/2$. For this wind, the compatible Fofonoff flow is characterized by a dominant northward anticyclonic

gyre, with the eastward return flow mainly along the northern boundary. A wind incompatible with Fofonoff flow is the double-gyre wind, $\tau_s = \sin(\pi y/L)$, corresponding to a westerly wind with a maximum at $y = L/2$. The solutions obtained with this wind (Fig. 3c) are similar to the classical double-gyre solutions studied by e.g. Holland (1978) and Marshall (1984).

The results of GS suggest that the nonlinear processes can largely be explained in terms of equilibrium statistical mechanics, that is the nonlinearity can be considered as a mixing process of the probability density function P in phase space, constrained by the integral conservation laws on E, Q_1 and Q_2. The validity of this viewpoint has been tested by GS introducing a stochastic model equation and comparing its solution with the solution of the quasi-geostrophic equation. We will come back on this point in the following.

3. Solutions with stochastic forcing. A general framework

In this section the results obtained by GS for steady winds are generalized to winds with a stochastic component. Some basic arguments are discussed here, that will be used in Section 4 to interpret a set of numerical experiments. Our main claim is that the stochastically fluctuating component of the wind always tends to induce an inertial circulation with a Fofonoff mean. This is due to the fact that the stochastic wind adds energy to the nonlinear eddy field, thereby increasing the nonlinear tendency toward the natural state characterized by the mean Fofonoff flow. To understand in which condition this tendency can actually be successful, we consider again the integral equation (2.9) considered in the case of steady wind. This equation has the same form as in the case with the steady wind alone, because the stochastic component of the wind has zero mean.

When the wind is purely stochastic (the steady component is zero, $\tau_s = 0$), Eq. (2.9) suggests that the natural tendency of the eddy field toward Fofonoff flow will be able to emerge, provided that the mean Fofonoff-like flow is completely supported by the eddy activity. The balance inside every closed streamline, in fact, must be between the eddy flux of q and the mean dissipation. We expect that the stronger is the stochastic forcing, the stronger is the eddy field and therefore the rectified mean flow.

When a steady component of the wind is present, we expect that the contribution of the stochastic component to the mean flow will be different depending on the geometry of the steady wind. Consider first the case of steady wind compatible with Fofonoff flow. The results of GS show that the solutions obtained with the steady wind alone have a strong mean flow similar to Fofonoff flow. The mean balance in (2.9), in the case of steady wind alone, is between the input of the wind and the dissipation, whereas the contribution of the eddy flux is negligible. When the stochastic component is added to the wind, the eddy field increases, increasing the nonlinear tendency toward the Fofonoff mean, in accordance with the mean induced

by the steady wind alone. We expect then that the resulting mean flow will have a structure similar to the one obtained with the steady wind alone, i.e. it will be Fofonoff-like, but it will be more energetic. In Eq. (2.9), the Reynolds flux will be increased with respect to the case with only steady wind, and, in effect, will serve to balance the increase in the dissipation term due to stronger vorticity in the mean flow. This picture qualitatively explains the results of Veronis, obtained with a fluctuating wind superimposed on a single-gyre steady wind, compatible with Fofonoff flow.

When the steady component of the wind is incompatible with Fofonoff flow, the situation changes. The stochastic wind still increases the nonlinear eddy field, but now the contribution of the eddies toward the Fofonoff flow is in opposition to the mean flow determined by the steady wind alone. As a consequence, we expect that the energy of the mean flow will not be increased, whereas the spatial structure of the solution is likely to be modified. The mechanisms that determine the modifications of the mean flow structure will be studied in Section 4 for a double-gyre solution. The results appear to be quite general and applicable to other wind geometries as well.

4. Numerical experiments

In this section, four numerical experiments are presented, obtained integrating numerically the quasi-geostrophic equation (2.1) with different wind forcings. The numerical model is the same as the one used in GS.

The action of the purely stochastic large-scale wind forcing, with no steady component, is studied in two experiments, ST1 and ST2, which differ only by the spatial structure of the stochastic wind. In ST1, the curl of the stochastic wind, curl τ_f, is characterized by an isotropic white wavenumber (K) spectrum with a cutoff at $K < 16/L$, where L is the basin scale. This representation is consistent with several observations (e.g. Frankignoul and Muller, 1979; Freilich and Chelton, 1985) that suggest a K^{-2} spectrum for the wind speed and wind stress, corresponding to a white spectrum for the curl of the wind. In ST2, instead, an unrealistically simple spatial structure, $\tau_f \propto \cos \pi y/L$, is chosen. The results of ST1 and ST2 are used to study the dependence of the solution on the space structure of the forcing. The time dependence of curl τ_f is modelled, for both ST1 and ST2, as a Markovian process in time (Treguier and Hua, 1987). The frequency (ω) spectrum is white, with white noise level W, for periods longer than 2Θ (where Θ is the integral time of the Markovian process) and it decays at shorter periods as ω^{-2}. This is in agreement with observations (e.g. Willebrand, 1978) that show a white frequency spectrum of the wind stress (and therefore of curl τ_f) at periods longer than a few days. The values of the integral time Θ and the white noise level W are chosen to be the same for the two experiments.

The effects of stochastic wind superimposed on a steady wind are investigated using the results of two experiments, 2GY and 2GYST1. They are characterized by

Table 1. Nondimensional parameters of the numerical experiments.

	$\epsilon/\beta L$ (10^{-4})	$\pi\tau_o/\rho H\beta^2 L^3$ (10^{-5})	$R = u_{rms}/\beta L^2$ (10^{-3})	E_{mf}/E
ST1	3.13		0.95	0.3
ST2	3.13		0.94	0.3
2GY	3.13	2.45	0.41	0.26
2GYST1	3.13	2.45	1.0	0.035

the same double-gyre steady wind, $\tau_s = \sin \pi y/L$, but in 2GY the stochastic component of the wind is zero, whereas in 2GYST1 it is the same as in ST1.

All the experiments are performed starting from the same random initial conditions. They are integrated in time until the solutions reach a statistical equilibrium, characterized by a constant value of the average total energy E. For all the solutions, the equilibrium is reached at approximately $1T_\epsilon$, where $T_\epsilon = 1/\epsilon$ is the drag decay time.

The main nondimensional parameters characterizing the four experiments are reported in Table 1. The first two rows give the nondimensional values of the decay coefficient ϵ and of the amplitude τ_o of the steady component of the wind stress. The following two rows identify the Rossby number $R = u_{rms}/\beta L^2$ of the solutions at equilibrium and the ratio between the energy of the mean flow, E_{mf}, and the total energy of the flow E. The dimensional values of the parameters of forcing and dissipation depend on the chosen values of β, H, L. For instance, if $\beta = 10^{-13}$ cm^{-1} sec^{-1}, $H = 4$ km and $L = 4000$ km, then $T_\epsilon = 2.54$ years, and $\tau_o = 2$ dyne cm^{-2}. The values of W and Θ, that are the same for ST1, ST2 and 2GYST1, are for this choice of the parameters $W = 10^{-7}$ N^2 m^{-6} Hz^{-1} and $\Theta = 3$ days. These values are of the same order of magnitude as the values used in other studies on the effects of stochastic wind (e.g. Treguier and Hua, 1987), and they are reasonable if compared to observations. Notice that the value used by WPP for W is lower by about one order of magnitude.

a. ST1 and ST2 experiments: Purely stochastic forcing. The two experiments ST1 and ST2, differing only in the spatial structure of the stochastic forcing, show very similar results in both the temporal evolution of the solutions and in the characteristics of the flows at the equilibrium. This indicates that the spatial structure of the forcing does not play an important role in determining the solutions. In the following, we discuss only the results of ST1, but a similar discussion could be made for ST2.

The initial evolution of ST1 is similar to the evolution observed in the free runs performed by GS. The energy and the enstrophy begin piling up in the western boundary, creating a strong western boundary layer, clearly visible in the mean flow computed over the first $0.1\ T_\epsilon$. As time progresses, the western intensification relaxes and boundary layers are formed along the zonal boundaries, reaching the eastern boundary at $\sim 0.25\ T_\epsilon$. At about $1\ T_\epsilon$ the solution is symmetric in the east-west

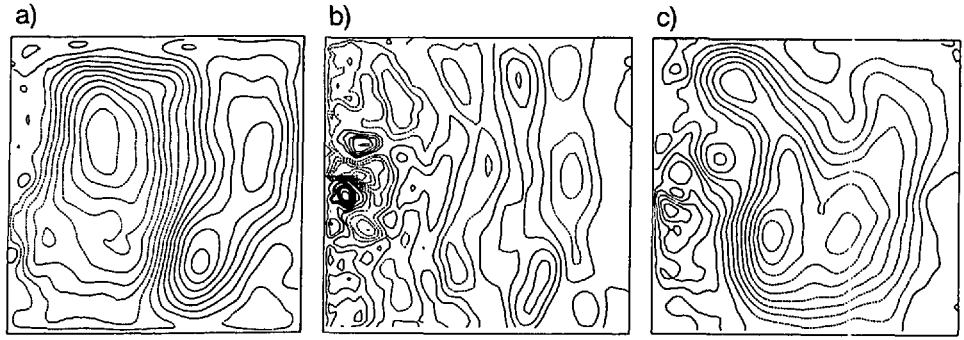

Figure 2. Instantaneous streamfunction for experiments (a) ST1; (b) 2GY; (c) 2GYST1.

direction and it appears to have achieved its equilibrium. We integrate the solution until 4 T_ϵ. A snapshot of ψ at 3.5 T_ϵ is shown in Figure 2a, whereas the mean $\langle\psi\rangle$ and $\langle q\rangle$, computed averaging over the last 1.5 T_ϵ are shown in Figure 3a, 3b. The ratio between the energy of the mean flow E_{mf} and the total energy E is $E_{mf}/E = 0.3$. The mean flow structure is very similar to the structure characteristic of the evolution of free tubulence (Fig. 1b). Two inertial gyres are evident, close to the zonal boundaries, an anticyclonic gyre in the north, and a cyclonic gyre in the south. As in the free solutions, the flow in the inertial gyres is characterized by a linear relationship between $\langle\psi\rangle$ and $\langle q\rangle$. These results confirm the arguments of Section 3, for which the stochastically driven solutions are expected to evolve toward a mean Fofonoff-like flow. The actual Fofonoff state is not reached and does not appear over the whole basin, because the dissipation arrests the evolution of the solution at a time comparable to T_ϵ, shorter than the time T_{eq} necessary to reach Fofonoff flow. An interesting difference between the free turbulence solutions and the stochastically driven solutions ST1 and ST2 is that the mean flow is stronger in the case of free turbulence. This can be easily understood considering (2.9). For the solutions ST1 and ST2, (2.9) states that a strong eddy flux of q is necessary in order to balance the bottom drag torque around each close streamline of the mean flow. This is not true in the case of free turbulence, as the bottom drag is zero.

In order to analyze the characteristics of the fluctuating field, we compute time series of the zonal and meridional velocities (u_1 and u_2 respectively) at three locations in the basin, indicated in Figure 4. Location 1 is in the western boundary layer, location 2 is in the interior and location 3 is in the southern boundary layer. In Figure 5a1–5a3, we show the spectra of u_2 at locations 1 and 2, and of u_1 at location 3. A narrow peak at high frequency is evident in all the spectra, corresponding to the frequency of 1,1 resonant Rossby basin mode computed from (Pedlosky, 1987)

$$\omega_{n,m} = \beta L/(2\pi(n^2 + m^2)^{1/2}).$$

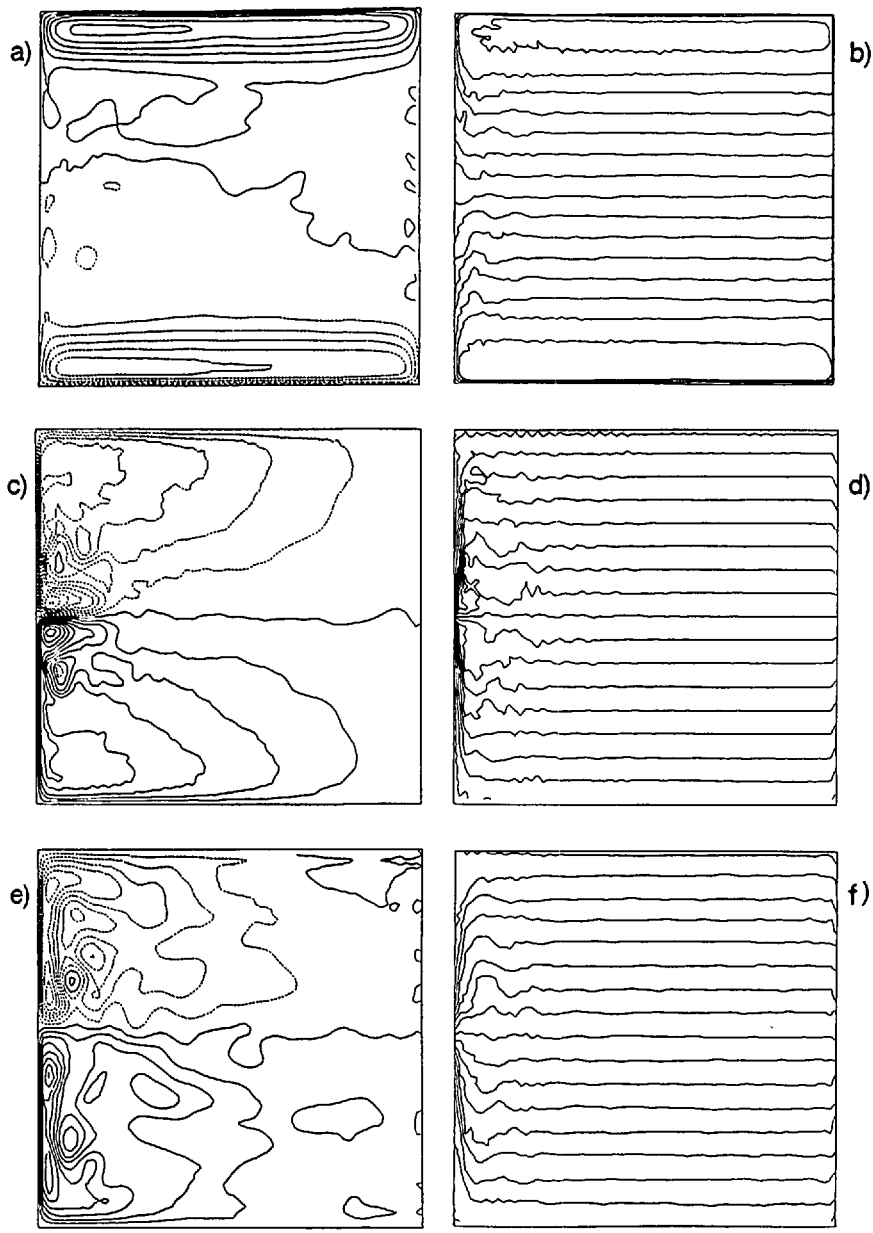

Figure 3. Average streamfunction (left) and potential vorticity (right) for experiments (a), (b) ST1; (c), (d) 2GY; (e), (f) 2GYST1.

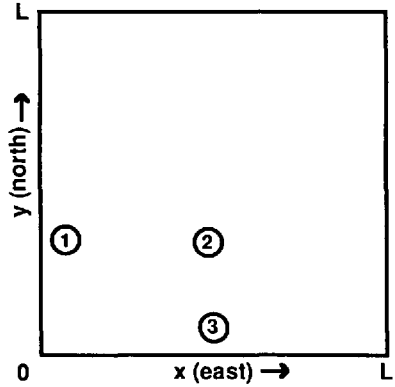

Figure 4. Locations of velocity measurements in the numerical experiments.

The corresponding dimensional period is $T_{1,1} \sim 15.8$ days, for the dimensional values mentioned above. A secondary peak can also be observed at lower frequencies, (dimensional period ~ 40 days). This peak is broader than the first one, especially in the interior, and it corresponds to higher normal modes which are not distinguishable one to another because of frictional effects.

It is interesting to compare the results of our experiments with the results of V70 and WPP. The regime considered by Veronis is characterized by higher forcing and dissipation than ours and his time-dependent forcing is not stochastic. WPP, instead, consider a less energetic forcing and higher friction, through a different mechanism (lateral friction). Nevertheless, both V70 and WPP observe the emergence of a mean flow qualitatively similar to the one that we observe. We interpret this result as evidence that the nonlinear tendency toward a Fofonoff-like mean flow is indeed very general. The more enhanced westward intensification present in the experiments of V70 and WPP with respect to our experiments is interpreted as due to higher dissipation, which stops the evolution of the inertial flow at an earlier stage. Also the spectral characteristics of the fluctuating field are similar in the experiments of WPP and in ours.

b. 2GY experiments: Steady forcing. The 2GY experiment has been performed using a steady forcing, $\tau_s = \sin \pi y$, opposing Fofonoff flow. The solution has been already discussed in GS. Here we summarize some of the main characteristics used as a reference to study the modifications that occur when a stochastic component is added to the wind.

The experiment has been run for 5.5 T_e. Figure 2b shows a snapshot of ψ at 3.8 T_e, whereas the mean $\langle\psi\rangle$ and $\langle q\rangle$, computed over the last 1.5 T_E are shown in Figure 3c, 3d. Both the value of the total energy E and the value of the ratio between E_{mf} and E ($E_{mf}/E = 0.26$) are lower than in the experiments ST1 and ST2. This indicates that the wind opposing Fofonoff flow is not very efficient in transferring energy to the

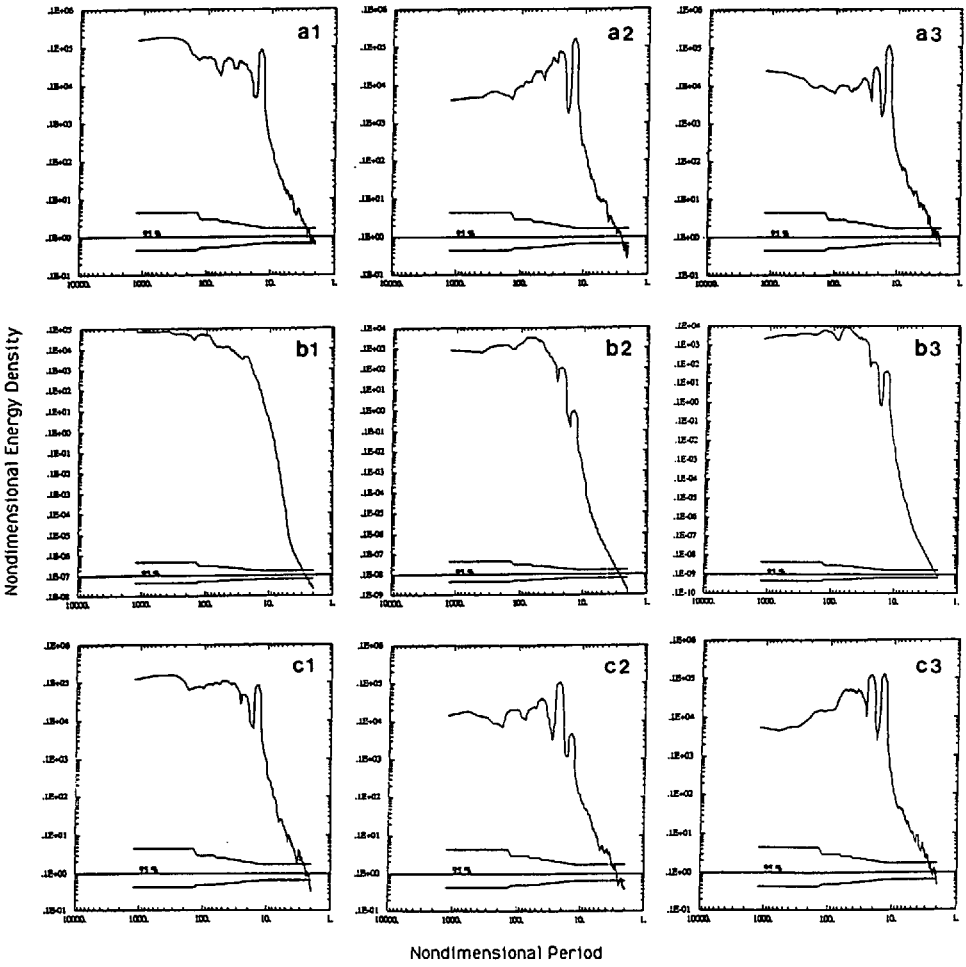

Figure 5. Velocity spectra at the three locations 1, 2, 3 shown in Figure 4, for the experiments (a) ST1; (b) 2GY; (c) 2GYST1. The energy density and the period are expressed in nondimensional units. For the values of the dimensional parameters given in Section 4, the units of the period are days.

ST1 experiment: (a1) meridional velocity at 1; (a2) meridional velocity at 2; (a3) zonal velocity at 3.

2GY experiment: (b1) meridional velocity at 1; (b2) zonal velocity at 2; (b3) zonal velocity at 3.

2GYST1 experiment: (c1) meridional velocity at 1; (c2) zonal velocity at 2; (c3) zonal velocity at 3.

ocean circulation, as already noted by GS. GS show that a steady wind with the same pattern and amplitude as in 2GY, but having opposite sign and therefore being compatible with Fofonoff flow, determines a much more energetic ocean response (more than 20 times). Here we see that also the purely stochastic wind is able to

induce an ocean circulation that is more energetic than the one induced by the steady wind opposing Fofonoff.

The mean flow in Figure 3c shows a cyclonic gyre in the northern basin and an anticyclonic gyre in the southern basin, characterized by strong western boundary currents and separated by a meandering jet, with intense recirculating regions at both sides. The potential vorticity q is homogeneous inside the recirculating regions. In order to study the dynamics of the solution, we compute the various terms of the averaged Eq. (2.8), integrated over the main dynamical regions of the flow. The interior of the gyres appears to be dominated by the linear Sverdrup balance. The western boundary layers are mainly inertial, with the β term balancing the advection of the mean ζ, $J(\langle\psi\rangle, \langle\zeta\rangle)$, whereas in the meandering jet and in the recirculating regions the advection of the mean ζ is balanced by the eddy advection, $\langle J(\psi', q')\rangle$. The formation of the unstable jet and of the recirculating regions can be explained as a consequence of conservation of q in the western boundary. In Lagrangian terms (Marshall, 1984), parcels of water circulating in the western boundary layers increase their relative vorticity ζ (positive in the northern gyre and negative in the southern gyre) while different latitudes are reached, in order to maintain q constant. When the particles arrive in the region that separate the two gyres, the excess of relative vorticity must be eroded, so that the particles can re-enter the linear interior. The meandering jet and the recirculating regions allow the process of erosion of relative vorticity to occur. The particles taken by the meandering jet, in fact, are exposed to regions of opposite-signed wind stress curl, and, as they recirculate, weak dissipation takes place. The turbulent particle motion inside the recirculating regions causes the potential vorticity to mix and consequently to homogenize (Cessi *et al.,* 1987).

The characteristics of the fluctuating field of 2GY have been studied using the spectra of u_2 at location 1 (in the western boundary layer), and of u_1 at locations 2 and 3, (in the interior and in the southern boundary layer) (Fig. 5b1–5b3). The western boundary spectrum is mainly red, due to the intense activity of eddies at various scales generated by current instabilities in the western region. The spectra in the interior and in the southern boundary layer, on the other hand, show two peaks corresponding to resonant Rossby modes. These occur at the same frequencies as in the ST1 spectra (Fig. 5a2, 5a3). This indicates that, as already pointed out by Miller *et al.* (1987), the ocean variability driven by fluctuating forcing and the variability due to mean flow instability have several similarities away from the western boundary. Notice, though, that the energy of the two peaks is lower in 2GY with respect to ST1, and that the relative size of the peaks is different in the two experiments. In ST1, where the fluctuation is driven by stochastic wind, the highest peak corresponds to the first resonant mode as predicted by linear theory. In 2GY, instead, where the fluctuation is forced by instability, the peak of the first mode is lower.

c. 2GYST1 experiment. Superposition of steady and stochastic forcing. The experiment 2GYST1 is driven by a superposition of the steady forcing of 2GY, $\tau_s = \sin \pi y/L$, and of the stochastic forcing of ST1. The forcing function is the only difference between 2GY and 2GYST1, so that the differences between the two experiments are solely due to the effects of the stochastic component of the wind.

The 2GYST1 experiment has been run for 5.5 T_ϵ. A snapshot of ψ at 4.8 T_ϵ is shown in Figure 2c, whereas the mean $\langle\psi\rangle$ and $\langle q\rangle$ computed over the last 2 T_ϵ are shown in Figure 3e, 3f. The total energy E of the flow is considerably higher than in the 2GY experiment, whereas the ratio E_{mf}/E is only 0.035, much lower than in 2GY. This indicates that, as discussed in Section 3, the stochastic forcing causes an increase in the eddy field of the solution (and therefore in the total energy), but the eddies do not contribute to reinforce the mean (recall that the mean here opposes Fofonoff flow).

The changes in the structure of the solution are studied in some details. It is evident from an inspection of Figure 3c and Figure 3e, that the major changes occur in the recirculating regions and in the meandering jet. They are less strong and less localized in 2GYST1 with respect to 2GY, and the potential vorticity inside the recirculating regions is not homogenized. To understand the different dynamics behind these changes, we compute the various terms of (2.8) integrated over the same regions as was done for 2GY. In the interior, the Sverdrup balance dominates, as in the 2GY experiment. In the western boundary layer, the eddy term $\langle J(\psi' q')\rangle$ is higher by about a factor 10 with respect to the value in 2GY. Its value is about half the value of the mean advection term, $J(\langle\psi\rangle, \langle\zeta\rangle)$. This indicates that in 2GYST1, contrary to 2GY, there is a substantial eddy flux of vorticity across the boundaries of the western boundary layer. The main balance is between the β term from one side and the sum of the eddy and the mean advection from the other side, whereas in 2GY the β term was balanced by the mean advection alone. As a consequence, the relative vorticity inside the western boundary does not increase with changing latitude as much as in the 2GY experiment, and therefore the intense region of instability at the gyre separation is not developed. In Lagrangian terms, the particles do not shoot straight along the western boundary current, but they are taken in a meandering path by the eddy field close to the western boundary. In this way, the excess of relative vorticity is not developed in the boundary layer, and the particles can re-enter the linear interior without going through the strong region of recirculation close to the gyre separation. The Sverdrup transport in the interior is not substantially altered by the stochastic wind.

It is interesting to compare the 2GYST1 experiment with the results of the SMb experiment of GS (Fig. 7d in GS), obtained integrating the stochastic model equation with the steady forcing alone. We recall that the stochastic model equation in GS is obtained from the quasi-geostrophic equation, substituting the advected vorticity

with a random variable, that tends to mix P in phase space, and maintaining only the gross conservation laws on E, Q_1 and Q_2. The detailed conservation of q following particles in absence of forcing and dissipation is not preserved by the stochastic model. The mean $\langle\psi\rangle$ and $\langle q\rangle$ of SMb show a clear resemblence with the corresponding means of 2GYST1. In SMb, as in 2GYST1, the recirculating regions and the jet between them are weaker than in 2GY and the potential vorticity q is not homogenized. The resemblance between SMb and 2GYST1 indicates that the action of the stochastic wind tends to increase the nonlinear process of mixing of probability density P in phase space, modifying mainly those characteristics of the solutions that are strictly related to the local dynamics of q. It is important to emphasize that the P mixing in phase space is a completely different process than the mixing of potential vorticity q in physical space, due to particle motion. The q mixing that occurs in the recirculating regions of 2GY causing the homogenization of q is actually weakened by the stochastic wind. As noted in Section 2, the nonlinear mechanism of P mixing in phase space is responsible for the tendency of the flow toward the statistical mechanics equilibrium characterized by the Fofonoff mean flow. The statistical mechanics equilibrium, in fact, is the state of maximum spreading of P in phase space at given values of $\langle E\rangle$, $\langle Q_1\rangle$ and $\langle Q_2\rangle$. The action of the stochastic wind can therefore be interpreted as increasing the tendency of the solution toward the statistical mechanics equilibrium.

The spectra of u_2 at location 1 (in the western boundary layer), and the spectrum of u_1 at location 1 and 3 (in the interior and in the southern boundary layer) are shown in Figures 5c1–5c3. In the western boundary, a clear peak is present at a frequency corresponding to the first resonant mode, in contrast to the 2GY spectrum. In the interior and in the southern boundary two peaks are present at the same frequencies as in the ST1 and 2GY spectra. As in 2GY, the peak corresponding to the first resonant mode is lower than the other peak. The energy of both peaks, though, is higher than in 2GY, and its level is similar to the level of ST1.

5. Conclusions

In this paper we study the action of the large-scale stochastic component of the wind on the climatological mean of the nonlinear ocean circulation, using a set of numerical solutions for the single-layer quasi-geostrophic equation with a flat bottom. We find that the effects of the stochastic component of the wind are strongly dependent on the presence of the steady component of the wind and on its geometry. When there is no steady component of the wind, the purely stochastic wind drives the quasi-geostrophic solutions toward a Fofonoff-like mean flow, similar to the mean flow that characterizes the evolution of the free turbulence solutions. The Fofonoff-like mean flow appears to be strong and does not depend on the details of the space structure of the stochastic wind. When a steady component of the wind is present, we argue that the stochastic wind tends to reinforce the mean solution obtained with the

steady wind alone, only if the steady wind is compatible with Fofonoff flow. When the steady wind opposes Fofonoff flow, instead, the contribution of the stochastic wind does not increase the energy of the solution, rather it tends to change the spatial structure of the mean solution. We study in detail the case of a stochastic wind superimposed on a double-gyre steady wind opposing Fofonoff flow. Since the double-gyre wind is an idealization of the real mean wind, this study provides indications on the effects of the synoptic wind activity on the general ocean circulation. We find that the energy and the Sverdrup transport of the ocean mean flow are not increased compared to the case of the steady wind alone. The mean flow energy is actually decreased. The stochastic wind, on the other hand noticeably changes the structure of the mean solution, especially in the highly nonlinear regions between the two gyres. The recirculating cells and the meandering jet between the gyres are weakened by the stochastic wind, and the homogenization of potential vorticity q inside the cells is inhibited. We compare the quasi-geostrophic solution with the solution of a stochastic model equation introduced by GS. The comparison indicates that the overall action of the stochastic wind can be understood as an increase in the mixing of the probability density function P in phase space. We note that the process of P mixing in phase space is distinct from the process of mixing of q in physical space. The q mixing is actually decreased by the stochastic wind, as indicated by the disappearance of the recirculating cells with constant q. The increase of the P mixing in phase space is a sign that the nonlinear eddy field, reinforced by the stochastic wind, tends more vigorously toward the natural, free equilibrium solution predicted by statistical mechanics. The double-gyre solution with stochastic wind can therefore be interpreted in terms of statistical mechanics equilibrium, even though the mean flow does not resemble Fofonoff flow.

An interesting aspect of our results is that they suggest a general methodology, applicable to models that are more complex and realistic than the simple quasi-geostrophic equation considered here. In analog to what was done for the quasi-geostrophic equation, the first step in the study of the response of a generic model equation to stochastic forcing should be the determination of its free equilibrium state, found by applying the method of equilibrium statistical mechanics. The free equilibrium state is, of course, dependent on the model, and it can be completely different from the Fofonoff flow. For instance, for a quasi-geostrophic flow with bottom topography, the free equilibrium state is characterized by a mean flow locked with the topography (e.g. Salmon, 1982). When the free equilibrium state is determined, it can be used to predict the tendencies of the forced and dissipative flows. As for the simple quasi-geostrophic flows considered here, we expect that a purely stochastic forcing would drive the nonlinear solutions of a generic model equation toward an equilibrium state with a mean similar to the one of the free equilibrium. In the presence of a steady component of the wind, the contribution of the stochastic wind is expected to depend on the geometry of the steady wind with respect to the

geometry of the free equilibrium state, in a similar fashion to what is described here. An interesting question that will be addressed in future work, is whether or not this mechanism also can be applied on a local basis. Consider, as an example, the single-layer quasi-geostrophic equation with bottom topography, forced by a steady wind superimposed on a stochastic component. Assume that the bottom topography is such that the steady wind is compatible with the free equilibrium mean (locked with topography) in some regions of the basin, whereas it is incompatible in other regions. If the response to the stochastic wind is local, then the mean flow due to the steady wind alone will become more energetic in the presence of the stochastic wind in the regions where the steady wind is compatible with the free equilibrium. In the other regions, the mean flow will not be strengthened, but it will be modified in its structure, according to the increase of P mixing in phase space determined by the stochastic wind.

Acknowledgments. The authors wish to thank G. Vallis for useful comments and criticism. This work was supported by the National Science Foundation, Grant #OCE9102604 and by the Office of Naval Research, Grant #N00014-91-J-1346.

REFERENCES

Barnier, B. and C. Le Provost. 1989. General circulation of the mid-latitude ocean: coupled effects of variable wind forcings and bottom topography roughness on the mean and eddy circulation, *in* Mesoscale/Synoptic Coherent Structures in Geophysical Turbulence, Proceedings of the 20th International Liege Colloquium on Ocean Hydrodynamics, J. C. J. Nihoul and B. M. Jamart, eds., Elsevier Science Publishers, 387–405.

Bretherton, F. P. and D. B. Haidvogel. 1976. Two-dimensional turbulence above topography. J. Fluid Mech., *78,* 129–154.

Carnevale, G. F. and J. D. Frederiksen. 1987. Nonlinear stability and statistical mechanics of flow over topography. J. Fluid Mech., *175,* 157–181.

Cessi, P., G. R. Ierley and W. R. Young. 1987. A model of the inertial recirculation driven by potential vorticity anomalies. J. Phys. Oceanogr., *17,* 1640–1652.

Dewar, W. K. 1989. A nonlinear, time-dependent thermocline theory. J. Mar. Res., *47,* 1–31.

Fofonoff, N. P. 1954. Steady flow in a frictionless homogeneous ocean. J. Mar. Res., *13,* 254–262.

Frankignoul, C. and P. Muller. 1979. Quasi-geostrophic response of an infinite β-plane ocean to stochastic forcing by the atmosphere. J. Phys. Oceanogr., *9,* 104–127.

Freilich, M. H. and D. B. Chelton. 1985. Wavenumber spectra of Pacific winds measured by the Seasat scatterometer. J. Phys. Oceanogr., *16,* 741–757.

Greatbatch, R. J. and J. Li. 1990. Barotropic variability in the presence of an ocean gyre. J. Mar. Res., *48,* 37–53.

Griffa, A. and R. Salmon. 1989. Wind-driven ocean circulation and equilibrium statistical mechanics. J. Mar. Res., *47,* 457–492.

Haidvogel, D. B. and P. B. Rhines. 1983. Waves and circulation driven by oscillatory winds in an idealized ocean basin. Geophys. Astrophys. Fluid Dyn., *25,* 1–63.

Holland, W. R. 1978. The role of mesoscale eddies in the general circulation of the ocean-numerical experiments using a wind-driven quasi-geostrophic model. J. Phys. Oceanogr., *8,* 363–392.

Holloway, G. 1986a. Eddies, waves, circulation and mixing: statistical geofluid mechanics. Ann Rev. Fluid Mech., *18,* 91–147.

—— 1986b. Comments on Fofonoff's mode. Geophys. Astrophys. Fluid Dyn., *37,* 165–169.

Kraichnan, R. H. and D. Montgomery. 1980. Two-dimensional turbulence. Rep. Progr. Phys., *43,* 547.

Marshall, J. 1984. Eddy-mean flow interaction in a barotropic ocean model. Q.J.R. Meteorol. Soc., *110,* 573–590.

Miller, A. J., W. R. Holland and M. C. Hendershott. 1987. Open-ocean response and normal model excitation in an eddy-resolving general circulation model. Geophys. Astrophys. Fluid Dyn., *37,* 253–278.

Muller, P. and C. Frankignoul. 1981. Direct atmospheric forcing of geostrophic eddies. J. Phys. Oceanogr., *11,* 287–308.

Pedlosky, J. 1987. Geophysical Fluid Dynamics, Springer-Verlag, NY, 626 pp.

Sadourny, R. and C. Basdevant. 1985. Parameterization of subgrid scale barotropic and baroclinic eddies in quasi-geostrophic models: Anticipated vorticity method. J. Atmos. Sci., *42,* 1353–1363.

Salmon, R., G. Holloway and M. C. Hendershott. 1976. The equilibrium statistical mechanics of simple quasi-geostrophic models. J. Fluid Mech., *75,* 691–703

Salmon, R. 1982. Geostrophic turbulence. Proc. Int'l. School of Physics Enrico Fermi., Varenna, Italy, 30–78.

Treguier, A. M. and B. L. Hua. 1987. Oceanic quasi-geostrophic turbulence forced by stochastic wind fluctuations. J. Phys. Oceanogr., *17,* 397–411.

Vallis, G. K., G. F. Carnevale and W. R. Young. 1989. Extremal energy properties and construction of stable solutions of the Euler equations. J. Fluid Mech., *207,* 133–152.

Veronis, G. 1970. Effect of fluctuating winds on ocean circulation. Deep-Sea Res., *17,* 421–434.

Willebrand, J. 1978. Temporal and spatial scales of the wind field over the North Pacific and North Atlantic. J. Phys. Oceanogr., *8,* 1080–1094.

Willebrand, J., S. G. H. Philander and R. C. Pacanowski. 1980. The oceanic response to large-scale atmospheric disturbances. J. Phys. Oceanogr., *10,* 411–429.

Received: *9 October, 1990;* revised: *30 January, 1991.*